Acta Crystallographica Section D
Biological Crystallography
ISSN 0907-4449

Hemoglobin redux: combining neutron and X-ray diffraction with mass spectrometry to analyse the quaternary state of oxidized hemoglobins

Timothy C. Mueser,[a]* Wendell P. Griffith,[a] Andrey Y. Kovalevsky,[b] Jingshu Guo,[a] Sean Seaver,[a] Paul Langan[a,b] and B. Leif Hanson[a]

[a]Department of Chemistry, University of Toledo, Toledo, OH 43606, USA, and [b]Bioscience Division, MS M888, Los Alamos National Laboratory, Los Alamos, NM 87545, USA

Correspondence e-mail: timothy.mueser@utoledo.edu

Received 17 April 2010
Accepted 28 June 2010

Improvements in neutron diffraction instrumentation are affording the opportunity to re-examine the structures of vertebrate hemoglobins and to interrogate proton and solvent position changes between the different quaternary states of the protein. For hemoglobins of unknown primary sequence, structural studies of cyanomethemoglobin (CNmetHb) are being used to help to resolve sequence ambiguity in the mass spectra. These studies have also provided additional structural evidence for the involvement of oxidized hemoglobin in the process of erythrocyte senescence. X-ray crystal studies of Tibetan snow leopard CNmetHb have shown that this protein crystallizes in the B state, a structure with a more open dyad, which possibly has relevance to RBC band 3 protein binding and erythrocyte senescence. R-state equine CNmetHb crystal studies elaborate the solvent differences in the switch and hinge region compared with a human deoxyhemoglobin T-state neutron structure. Lastly, comparison of histidine protonation between the T and R state should enumerate the Bohr-effect protons.

1. Introduction

To describe hemoglobin as well studied seems an understatement, especially to crystallographers. With the recent festivities commemorating the 50th anniversary of the MRC and the determination of the structures of myoglobin and hemoglobin, the importance of these proteins to the development of structural biology seems unlikely to be forgotten. What may be less known is the role played by heme proteins in the development of neutron protein crystallography. The determination of the position of H atoms about the heme group in myoglobin first led Benno Schoenborn to attempt neutron diffraction on proteins (reviewed in Schoenborn, 2003). We recognize our debt to Benno, both for pioneering neutron diffraction of proteins and for providing us specifically with insight into hemoglobin preparation and crystallization. In addition, we also wish to recognize our debt to the Medical Research Council Laboratory of Molecular Biology at Cambridge that helped to pioneer so much of structural biology. For two of us (TCM and BLH) the debt is personal, as our mentors Arthur Arnone and Allen Edmundson were part of the hemoglobin and myoglobin efforts at the MRC.

To date, arguably the greatest impact of neutron protein crystallography has been made in understanding enzyme structure and function. Discussed elsewhere are insights into the catalytic function of D-xylose isomerase (Kovalevsky, Hanson *et al.*, 2010), DFPase (Blum *et al.*, 2009), dihydrofolate reductase (Bennett *et al.*, 2006), endothiopepsin (Tuan *et al.*, 2007; Coates *et al.*, 2008), aldose reductase (Hazemann *et al.*, 2005; Blakeley *et al.*, 2008) and human carbonic anhydrase II

(Fisher *et al.*, 2009, 2010) based on neutron diffraction studies. However, neutron diffraction can provide useful insight into most proteins and hemoglobin is a prime candidate for structural elucidation using this technique. Neutrons provide direct experimental visualization of the H atoms and protons in a protein. In contrast, with X-rays the H atom scatters X-ray photons feebly, while H^+ is not visible. For hemoglobin, neutron diffraction is especially advantageous. Hemoglobin is reliant on His side chains for hydrogen-ion buffering, blood CO_2-transport capacity and the molecular mechanism for the reduced affinity for oxygen at low pH, the Bohr effect. The neutron structure of the human deoxy state of the protein has been completed (Chatake *et al.*, 2007; Kovalevsky *et al.*, 2008; Kovalevsky, Chatake *et al.*, 2010), facilitating comparison between the unliganded and liganded forms of the protein.

The contribution of His side chains to the Bohr effect has still not been fully resolved. Early studies by Perutz suggested a limited number of Bohr groups that are essentially conserved in vertebrate hemoglobins (Perutz, 1983). However, more recent NMR work has suggested that a larger number of His side chains contribute to the Bohr effect (Lukin & Ho, 2004; Berenbrink, 2006). In addition, solvent motion and displacement mediate quaternary-structure changes in hemoglobin. In the transition from deoxygenated to oxygenated conditions [classically labeled the tense (T) and relaxed (R) states, respectively], there is now clear evidence that the dimer–dimer interface of liganded hemoglobin has a wide range of energetically accessible structures that are related to each other by a simple sliding motion (Mueser *et al.*, 2000). The dimer–dimer interface acts as a 'molecular slide bearing' that allows the two dimers to slide back and forth without greatly altering the number or the nature of the intersubunit contacts. Solvent plays an essential role in this interface sliding (Mueser *et al.*, 2000) and mediation of T *versus* R interconversion. The role of His side chains in the Bohr effect can be understood as either a limited number of side chains providing strong links to stabilize the T state (the Perutz model) or the aggregative and concerted effect of His-residue protonation stabilizing the T state (the Lukin and Ho model). In either case, knowledge of hydrogen position and protonation states is essential to our understanding of hemoglobin function.

More recently, greater insight has been sought into erythrocyte-senescence processes and how this knowledge can improve the effectiveness of blood transfusion (Kriebardis *et al.*, 2007). Across vertebrate taxa, erythrocytes have markedly different life spans. Human and canid red cells have an *in vivo* life span of the order of 120 d and rat and mouse red cells of approximately 40–60 d, while box turtle and South American giant toad red blood cells have life spans of 600–800 and 700–1400 d, respectively (Altland & Brace, 1962). Our interest is to elucidate the role of divergent evolution of primary sequences of a wide variety of vertebrate hemoglobins along with their cognizant N-terminal domains of the erythrocyte chloride/carbonate-ion transporter, the band 3 protein. As a carrier of oxygen, the ferrous heme (Fe^{2+}) transiently binds molecular oxygen, releasing the ligand in response to the lowering of oxygen tension in the capillaries. It has long been known that as anuclear red cells age there is increased formation of ferric methemoglobin (Fe^{3+}) and hemichrome, both of which bind more strongly to the Hb-binding domain of band 3 (the N-terminal 40 residues) than oxy- (R-state) or deoxy- (T-state) Hb (Waugh & Low, 1985). The evolution of this oxidized Hb–band 3 interaction is one of the progenitors of erythrocyte aging and subsequent removal from the body. This binding of hemoglobin to band 3 initiates a cascade of events, including the clustering of band 3 in the cell membrane, restructuring/reorganization and destabilization of the membrane and the formation of a binding site for IgG autoantibody, which triggers the removal of the red cell from the body (Low, 1991). The vastly varying life spans of red cells across nature may be a consequence of differences in the sequences of Hb and its cognate band 3 and correlated with the strength of the interactions between these two important proteins.

There is a large database of primary sequences of human hemoglobin mutants available, especially those associated with hemoglobinopathies (HbVar, http://globin.cse.psu.edu/hbvar/menu.html). While the sequences of many vertebrate Hbs have been determined, the fraction of species known is relatively small. In our studies, mass spectrometry (MS) plays a major role in the determination of these Hb sequences. With the development and growth that MS technology and computer processing power have seen in recent years, MS has become the cornerstone of protein sequencing. Using the so-called 'bottom-up' approach, the purified protein of interest is digested by an endoproteinase (commonly trypsin) and the resultant peptides are injected into the mass spectrometer, fragmented and the masses of the intact peptides and fragments are recorded. Using computing methods such as *de novo* sequencing, peptide-map fingerprint searching and sequence-homology searches, a sequence of the protein can be constructed. One major problem associated with this MS approach is that complete sequence coverage cannot be achieved. Another problem that plagues MS protein sequencing is the presence of isomeric (leucine and isoleucine) and isobaric (glutamine and lysine) residues. Without a very high resolution and highly mass-accurate mass spectrometer, it is almost impossible to differentiate between glutamine and lysine in a simple MS experiment. Also, the isomeric leucine and isoleucine have the same mass and can only be differentiated by the analysis of side-chain fragments, which is not a trivial task. After digestion, in many cases some of the resultant peptides are too small (*e.g.* monopeptides, dipeptides, tripeptides), too large to provide fragments representative of the entire peptide sequence after tandem MS or too hydrophobic to provide reasonable ionization efficiency for detection. These all result in decreased sequence coverage by the bottom-up MS approach.

By exploiting the unique propensity of hemoglobin to crystallize, regardless of species, combined with high-resolution mass spectrometry, we are able to achieve 100% coverage of hemoglobin protein sequences. For the few cases completed thus far, we have used mass spectrometry to determine as much of the protein sequence as possible. This is

typically around 70–90%. Sequence information from MS is then used in molecular-replacement phasing and refinement of the crystal structure. Electron-density maps can then be used to differentiate between leucine and isoleucine and between glutamine and lysine. The electron-density maps can also be used to fill in all of the blanks left in the MS-determined sequence. The power of the complementarity of mass spectrometry and protein crystallography is that while in crystal structures with low- to average-resolution data it is difficult to impossible to differentiate between residues with similar shapes (aspartate/asparagine, glutamate/glutamine, valine/threonine), these are extremely easily differentiated using mass spectrometry. Although the purpose of using crystallography for the studies described here was to determine the sequences of proteins, it is quite clear that this role is most easily and effectively accomplished in concert with mass-spectrometric analysis.

Our preliminary studies have been directed towards sequence and X-ray structure determination of Tibetan snow leopard cyanomethemoglobin (CNmetHb) and determination of the neutron and X-ray structures of equine CNmetHb. We chose to use CNmetHb for protein stability; however, the choice proved to be serendipitous, as snow leopard CNmetHb had a quaternary structure that could have implications for RBC senescence.

2. Experimental methods

2.1. Protein isolation

Uncia uncia (Tibetan snow leopard) packed red blood cells (pRBC) were generously donated for research purposes by the Toledo Zoo (Toledo, Ohio, USA). These samples are usually discarded as waste during the collection of serum from the animals for routine hormone and other diagnostic testing. Equine pRBC were obtained from a local veterinary facility. Proteomics-grade TPCK-treated trypsin, NaCN and $K_4Fe(CN)_6{\cdot}3H_2O$ were purchased from Sigma Chemical Co. (St Louis, Missouri, USA). Sephadex G25 resin was obtained from GE Healthcare. The hemoglobin crystal screening kit was prepared as described by Mueser *et al.* (2000). All other chemicals, buffers and solvents were of analytical grade or higher. Microcon centrifugal filters with 10 kDa cutoff were obtained from Millipore (Billerica, Massachusetts, USA).

2.2. Preparation of CNmetHb and isolation from pRBCs

Snow leopard and equine pRBCs were suspended three times into a 10× volume of phosphate-buffered normal saline (0.09 *M* NaCl, 0.01 *M* sodium phosphate pH 7.4) and centrifuged at 2000*g* for 10 min at 277 K to rinse the red cells. The buffy coat was removed by aspiration. The rinsed cells were suspended in a 3× volume of phosphate buffer (0.005 *M* sodium phosphate pH 7.4) to induce osmotic lysis. The lysed cells were then subjected to high-speed centrifugation at 16 000*g* for 15 min at 277 K to separate the hemolysate, which contains almost pure hemoglobin, from the erythrocyte ghost membrane fraction. Hemoglobin solutions were treated with buffered ferricyanide/cyanide [10 m*M* $K_4[Fe(CN)_6]{\cdot}3H_2O$, 2 m*M* NaCN, 10 m*M* Tris–HCl pH 7.4] and eluted from a 20× volume home-packed column of Sephadex G25 (GE Healthcare) using 10 m*M* Tris–HCl pH 7.4 to remove excess ligand and hemichrome. CNmetHb solutions were concentrated using Microcon YM-10 centrifugal concentrators. The concentrations of hemoglobin solutions were determined using UV–Vis absorbance ($C = A_{540\,\mathrm{nm}} \times 1.465$, where C is in mg ml^{-1}; International Committee for Standardization in Haematology, 1978). The product equine CNmetHb was further purified on a desalting column (Sephadex G25) against 10 m*M* HEPES pH 7.2 and was concentrated to 40 mg ml^{-1}.

2.3. Globin-chain chromatography and digestion

Globin-chain isolation was performed by reversed-phase HPLC on a Shimadzu Biotech Prominence HPLC (Columbia, Maryland, USA) equipped with a dual-wavelength detector. 20 µl of approximately 1 mg ml^{-1} Hb solution was applied onto a 4.6 × 100 mm BDS Hypersil C18 analytical column with 3 µm particle size (Thermo Electron Corp.). Solvent *A* consisted of 0.1% trifluoroacetic acid (TFA) in water and solvent *B* consisted of 0.1% TFA in acetonitrile (ACN). For all separations, the flow rate used was 1 ml min^{-1}. Absorbance was measured at 280 and 214 nm. For the snow leopard Hb, globin separation was achieved using an optimized elution-gradient profile from 35% *B* to 60% *B* over 25 min. The identities of the representative peaks for the α and β chains were confirmed by electrospray ionization mass-spectrometry (ESI-MS) measurements. The pooled fractions were evaporated to dryness by Speedvac at 303 K.

Pooled fractions containing purified globin chains were reconstituted by dissolution in 100 m*M* ammonium bicarbonate pH 8.5 and digested with proteomics-grade trypsin using an approximately 1:50 molar ratio of enzyme to globin chain. Incubation was carried out at 310 K overnight.

2.4. Mass spectrometry

Mass-spectrometric data were collected on a Synapt HDMS quadrupole–time-of-flight ion-mobility mass spectrometer equipped with a nanospray source (Waters Corp.). Instrument parameters were maintained at the following values for each experiment: capillary voltage, 3.0 kV; sample cone, 40 V; cone gas, 0 l h^{-1}; trap collision energy, from 6 V (for intact globin mass measurement) to 30 V (for peptide MS/MS). Mass spectra were calibrated externally in the range $50 \leq m/z \leq 3000$ using a solution of sodium caesium iodide and were processed using *MassLynx* 4.1 software (Waters). All mass spectra were averages of 300 scans and are presented unprocessed (unsmoothed and without background subtraction). All globin samples (intact or digested) were reconstituted in a solution containing 0.1% formic acid and 50% ACN and diluted to working solution concentrations of approximately 2–10 µ*M*.

For the bottom-up sequencing of the tryptic peptides, after a mass spectrum representative of the digest mixture of tryptic peptides had been acquired, each peptide was isolated, frag-

Table 1
X-ray diffraction data measurement statistics.

	Snow leopard CNmetHb	Equine CNmetHb
Space group	$P2_1$	$C2$
Unit-cell parameters (Å, °)	a = 54.4, b = 74.9, c = 75.6, β = 104.7	a = 108.9, b = 63.2, c = 54.7, β = 110.7
Resolution (Å)	43.05–2.10 (2.18–2.10)	31.58–1.70 (1.76–1.70)
No. of measured reflections	95957	137874
Unique reflections	33853 (3285)	36049 (3351)
Redundancy	2.83 (2.37)	3.82 (3.77)
Completeness (%)	98.4 (89.2)	94.3 (90.8)
$\langle I/\sigma(I)\rangle$	11.0 (3.1)	10.9 (2.1)
$R_{\rm merge}$†	0.053 (0.238)	0.058 (0.348)

† $R_{\rm merge} = \sum_{hkl}\sum_i |I_i(hkl) - \langle I(hkl)\rangle| / \sum_{hkl}\sum_i I_i(hkl)$.

mented by collision-induced dissociation and tandem mass spectra were recorded in the m/z range 50–3000. Data were searched against the Protein Data Bank using the online *MASCOT* utility (available at http://www.matrixscience.com). The sequence homology of globin hits from the *MASCOT* search was used to facilitate compilation of the protein sequence from peptide MS and MS/MS data.

2.5. Crystallization

2.5.1. Crystallization of snow leopard CNmetHb. A 20 mg ml^{-1} solution of snow leopard CNmetHb was used to screen for crystallization conditions using the hanging-drop method. Crystals of snow leopard CNmetHb were obtained at room temperature using a mother liquor consisting of 0.2 *M* sodium cacodylate, 0.1 *M* PIPES pH 6.5 and 14% PEG 4000.

2.5.2. Crystallization of equine CNmetHb. Crystallization of equine CNmetHb for neutron studies was carried out in H_2O according to the batch method. Crystallization drops of 500–800 µl in volume were set up in a nine-well glass plate (Hampton Research) sealed with CrystalClear tape (Hampton Research). Crystals of the order of 5–10 mm^3 in volume normally grew within a month at 290 K from drops consisting of 5 m*M* HEPES, 20 mg ml^{-1} equine CNmetHb and 40% saturated ammonium sulfate adjusted to pH 7.2 with NaOH.

2.6. Diffraction data measurement

2.6.1. Snow leopard CNmetHb. Diffraction data for snow leopard CNmetHb were measured at 100 K at NE-CAT at APS, Argonne National Laboratory. Cryoprotection for the snow leopard CNmetHb crystals was provided by adding PEG 400 to a volume of 12% of the crystallization buffer. The data were processed using *MOSFLM* (Leslie, 1992) and molecular replacement and refinement is under way using the *CCP*4 suite of programs (Collaborative Computational Project, Number 4, 1994). Diffraction data statistics are shown in Table 1.

2.6.2. Equine CNmetHb. The 293 K X-ray crystallographic data set was measured to 1.7 Å resolution in-house from a crystal of equine CNmetHb sealed in a thin-walled quartz capillary with D_2O buffer using a Rigaku FR-E diffractometer equipped with an R-AXIS VI^{++} detector. Diffraction data were integrated and scaled using the *CrystalClear*/*d***TREK* software (Pflugrath, 1999) and structure refinement is in progress using *SHELX* (Sheldrick, 2008). Equine CNmetHb crystallized in space group $C2$, with unit-cell parameters a = 108.86, b = 63.16, c = 54.71 Å, β = 110.75°. Further diffraction statistics can be found in Table 1 and in Kovalevsky, Fisher *et al.* (2010).

For neutron diffraction, several candidate crystals were successfully mounted in quartz capillaries that were reshaped with a CH_4/O_2 torch to give an hourglass constriction in order to prevent the crystal from slipping during the diffraction experiment. Deuterated buffer (∼0.5 ml) was placed in the lower part of the capillary. H/D vapor exchange was allowed to occur in the capillary for one month before the collection of

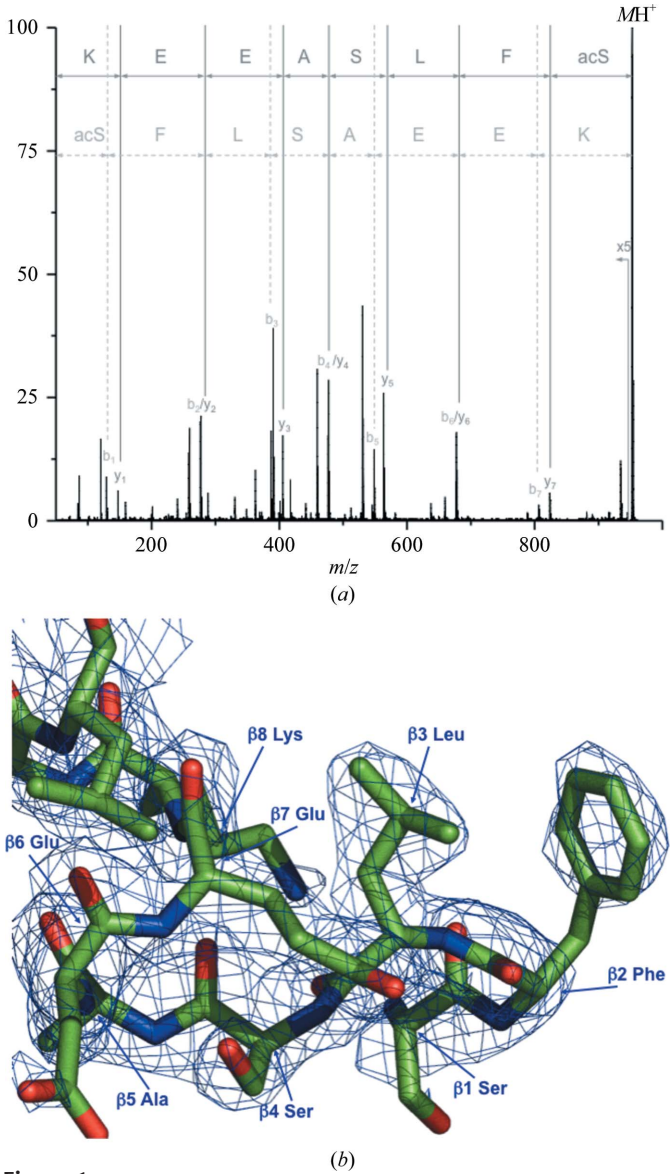

Figure 1
Deconvolution of sequence ambiguity from mass spectra using X-ray crystallography. (*a*) Mass spectrum for the N-terminal peptide fragment of snow leopard Hb β chain. The top line reading from right to left is the sequence. The identity of the third residue is ambiguous. (*b*) Electron density (contoured at 1.5σ) of the β-chain N-terminus. The density for the third residue indicates that Leu is the appropriate choice.

neutron diffraction data. A 17 h test exposure was taken from the largest equine CNmetHb crystal (~10 mm^3), yielding diffraction to better than 2.0 Å resolution.

Time-of-flight wavelength-resolved Laue images were measured at room temperature on a Huber κ-circle goniometer at 37 usable settings, with approximately 17 h exposure times per diffraction image, at the Protein Crystallography station at LANSCE (Los Alamos National Laboratory). The crystal-to-detector distance was set to 730 mm, corresponding to the cylindrical radius of the detector, while the detector was normally kept at $2\theta = 0^\circ$ during the entire experiment, effectively collecting data in the $\pm 60^\circ$ 2θ range. Because of the narrow $\pm 8^\circ$ span of the detector in the vertical direction, the crystal had to be reoriented eight times using the κ and ω goniometer circles and φ scans performed at each crystal orientation. Each image was processed using a version of *d*TREK* (Pflugrath, 1999) modified for wavelength-resolved Laue neutron protein crystallography (Langan & Greene, 2004). The integrated reflections were wavelength-normalized using *LAUENORM* (Helliwell *et al.*, 1989) and then merged using *SCALA* as incorporated in the *CCP*4 program suite (Evans, 2006; Weiss, 2001; Diederichs & Karplus, 1997; Weiss & Hilgenfeld, 1997; Collaborative Computational Project, Number 4, 1994). The 'tails' of the wavelength range were cut off slightly, to a restricted range of 0.72–6.25 Å, from the original 0.6–7.0 Å wavelength distribution of the neutrons in order to eliminate the least accurately measured reflections. The overall completeness was 80.2% to 2.0 Å resolution, with an $R_{\rm merge}$ of 0.242 and a multiplicity of 2.7 for the low-symmetry space group *C*2.

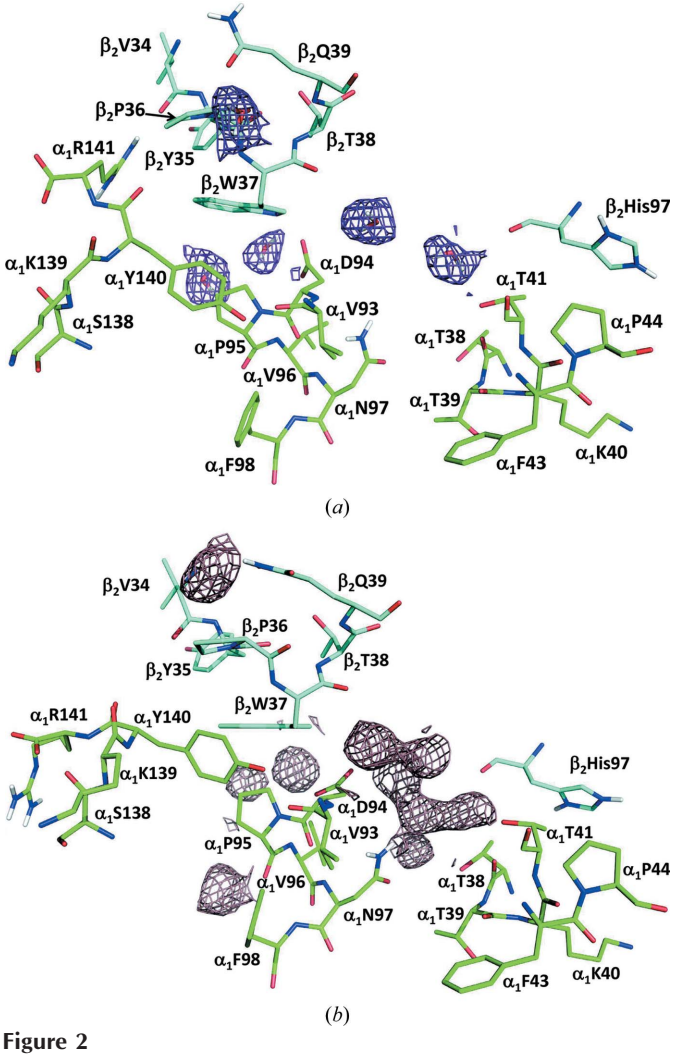

Figure 2
Contrasting neutron density (contoured at 1σ) near the switch and hinge regions of T-state and R-state hemoglobin. (*a*) T-state human deoxyhemoglobin; (*b*) R-state equine cyanomethemoglobin.

3. Results

3.1. Sequence determination using mass spectrometry and X-ray diffraction

A representative peptide-fragment mass spectrogram from the N-terminus of the β chain of snow leopard Hb is shown in Fig. 1(*a*). Owing to the nature and nomenclature of peptide fragments in tandem mass spectrometry, when using y-ions (C-terminal fragment ions) the peptide sequence should be read from right to left, showing an Ile/Leu ambiguity at position 3.

A molecular-replacement solution for snow leopard CNmetHb was found and an initial model was made based on the human recombinant hemoglobin 1.1 model 1aby (Kroeger & Kundrot, 1997). After mutation of the sequence with the available mass-spectrometry results for snow leopard hemoglobin, OMIT maps were made of regions of sequence ambiguity. As can be seen in Fig. 1(*b*), it is relatively straightforward to assign Leu or Ile based on electron density.

3.2. X-ray and neutron diffraction of equine CNmetHb

A molecular-replacement solution for equine CNmetHb was found and an initial model was made based on the equine carbonmonoxyhemoglobin model 1g0b (Mueser *et al.*, 2000). Joint X-ray–neutron (XN) refinement of the structure is currently in progress utilizing the program *nCNS* (Adams *et al.*, 2009) modified from the original *CNS* (Brünger *et al.*, 1998) including both 293 K neutron and 293 K X-ray reflection files in the refinement. Initial neutron density maps calculated after rigid-body refinement and one round of positional and *B*-factor refinement show the clear features that are usually observed for neutron maps. D atoms on exchangeable groups such as OH and NH are clearly visible as strong nuclear density peaks. H atoms are detected as troughs in the negative $2F_{\rm o} - F_{\rm c}$ nuclear density map. These are attached to non-exchangeable aliphatic and aromatic groups and have a negative scattering length for neutrons. Solvent can be readily observed and the orientations of the water molecules can be determined (Fig. 2).

4. Discussion and future studies

4.1. Unanticipated differences in CNmetHb

The initial model of snow leopard CNmetHb was a surprise. Rather than the spherical morphology of T-state and R-state

hemoglobin, the quaternary structure was more elliptical. After comparing this structure with hemoglobin structures in the PDB, a similar morphology was found for 1aby, a human recombinant hemoglobin structure solved by Kroeger & Kundrot (1997), who described this quaternary morphology as B state. In this B-state recombinant protein, the α chains are fused in an attempt to reduce tetramer dissociation, thereby reducing renal clearance of this potential blood substitute. The α-chain fusion was thought to elicit the new B-form quaternary state. Here, we find the B state in normal oxidized vertebrate hemoglobin. The two B-state models are shown in ribbon-diagram representations in Fig. 3. The deoxy T state has a large central opening along the molecular dyad, whereas the liganded R-state central cavity is more closed. A band 3 N-terminal peptide cocrystallized with human deoxy T-state hemoglobin appears bound in the BPG binding site along this central dyad (Walder *et al.*, 1984). The snow leopard B-state hemoglobin, despite being liganded, has a central cavity that is significantly larger than that of the T state (see Fig. 4*b*). As mentioned earlier, denatured and unstable hemoglobins and hemichromes bind the N-terminus of RBC band 3 protein more tightly. We are therefore currently exploring the affinity between oxidized B-state hemoglobin and the band 3 N-terminal sequence of various vertebrate species.

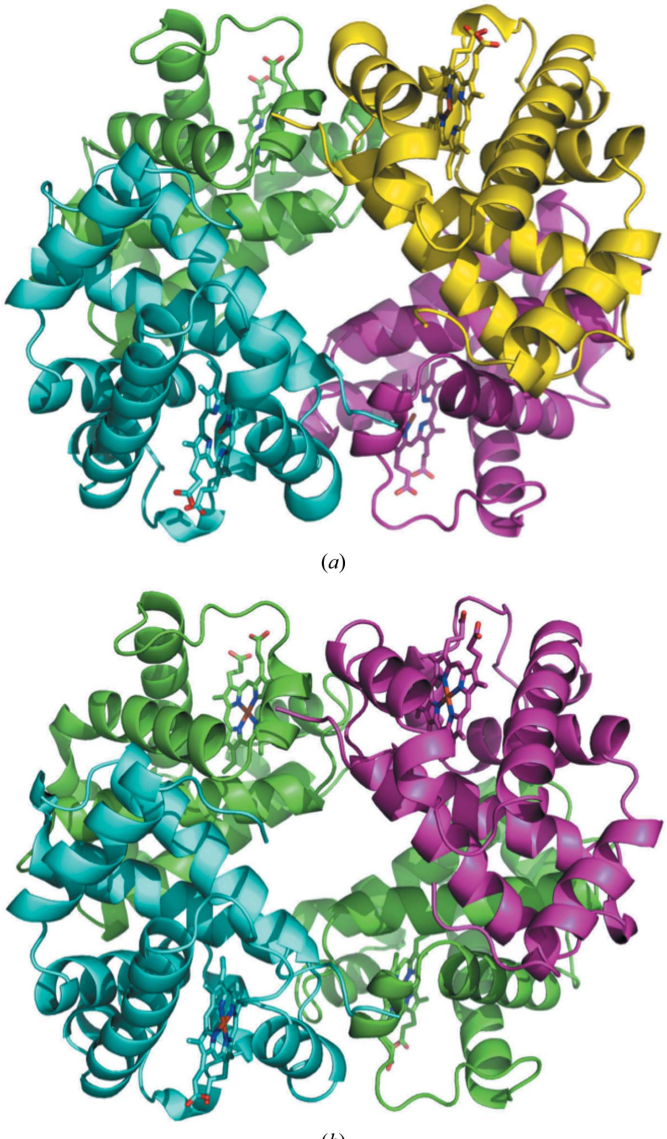

(*a*)

(*b*)

Figure 3
Ribbon backbone models for two different B-state hemoglobins: (*a*) snow leopard CNmetHb, (*b*) human recombinant 1.1 CNmetHb.

4.2. Differences in R-state and T-state neutron structures

Neutron diffraction is becoming the pre-eminent technique to determine residue protonation and protein solvation. Despite being in the early stages of model building and molecular refinement, the neutron diffraction structure of equine CNmetHb can provide insight into solvation changes

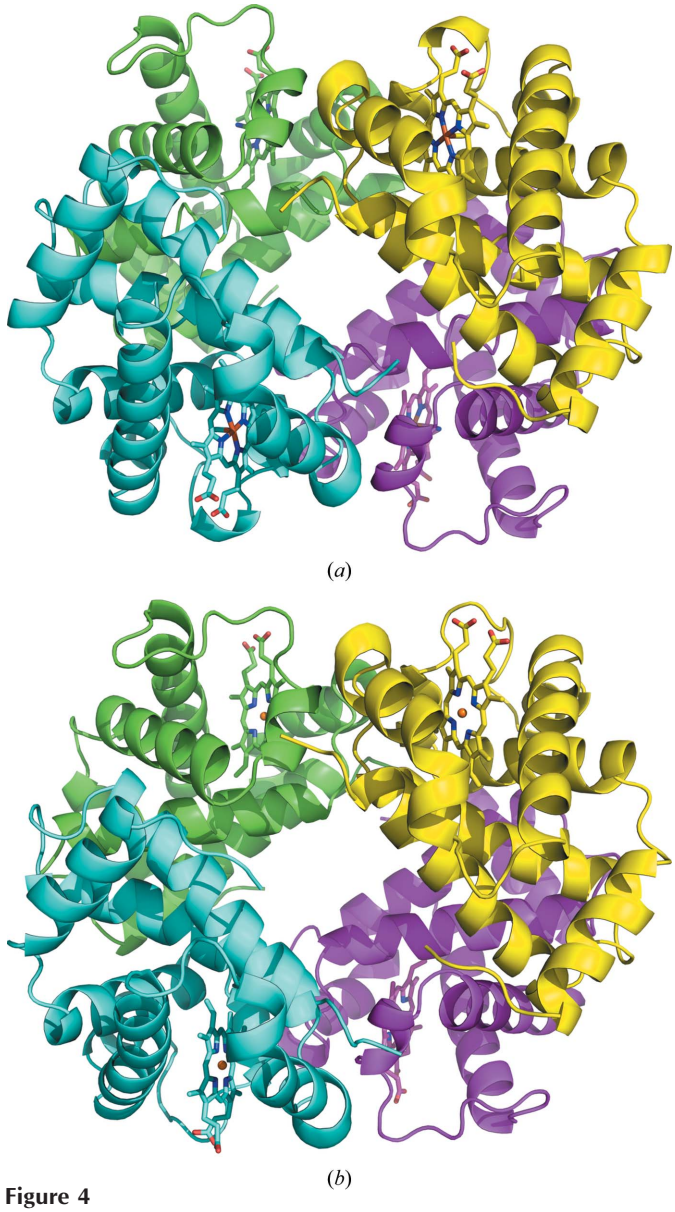

(*a*)

(*b*)

Figure 4
Ribbon backbone models of R-state and T-state hemoglobin. Note the larger central opening for the T state, which is comparable to the larger opening seen in the B state (Fig. 3). (*a*) Equine CNmetHb, (*b*) human deoxyhemoglobin.

in hemoglobin, especially when compared with the neutron structure of human deoxyhemoglobin. We anticipated changes in the hinge and switch regions as a consequence of the transition from the T to the R state. In Fig. 2, the increase in solvent is clearly seen in the R-state model, especially in the region between the hinge and the switch. Although not as readily seen in this figure, there appears to be a motion of water near the α chain Pro95 towards the solvent between the hinge and the switch, which is consistent with our previous studies (Mueser *et al.*, 2000). This region is close to the heme and increased solvation is correlated with decreased O_2 affinity of the hemoglobin. One additional feature that we see in our hemoglobin-solvation studies is the expulsion of a water molecule from near the heme when equine CNmetHb diffraction is measured at 100 K (Kovalevsky, Fisher *et al.*, 2010). Whether this water molecule is displaced as a consequence of the cryoprotection conditions will be determined from room-temperature studies of cryoprotected crystals. With respect to protonation, Hisβ97 is clearly doubly protonated in both structures despite the increased solvation near this residue and the pH 7.2 crystallization conditions for the R state.

4.3. Future studies

Efforts are currently under way to complete joint X-ray and neutron structural refinement of equine CNmetHb. One of the primary goals of the completed structure will be to compare the protonation differences of the His residues between the T and R states to help to enumerate the Bohr-effect histidines. Neutron diffraction studies of B-state hemoglobin should also provide an interesting comparison with R-state and T-state interfaces. We are currently crystallizing CNmetHb from the Amur tiger (*Panthera tigris altaica*) for neutron diffraction. The habit of Amur tiger CNmetHb crystals is cuboid and large single crystals well suited for neutron studies are formed. The sequence of Amur tiger hemoglobin has been determined and molecular models based on preliminary diffraction studies indicate that the CNmet form of the protein is also B-state.

Production of mass spectra of hemoglobin to determine the amino-acid sequence continues and isolation of the RBC band 3 proteins from the diverse taxa for which we have blood samples is beginning. Affinity-constant determination for band 3 N-termini and selected hemoglobins are planned, as is the determination of the affinity of the band 3 N-terminal peptide for B-state hemoglobin. Despite decades of structural studies with hemoglobin, there is still a surprising amount of information yet to be gleaned.

The PCS is funded by the Office of Biological and Environmental Research of the US Department of Energy. TCM, SS and BLH were supported by NSF (446218). PL was partly supported by an NIH–NIGMS-funded consortium (1R01GM071939-01) between LANL and LBNL to develop computational tools for neutron protein crystallography. AYK was partly supported by a LANL LDRD grant (20080789PRD3). AYK and PL were partly supported by a LANL LDRD grant (20070131ER). This work is based upon research conducted at the Advanced Photon Source on the Northeastern Collaborative Access Team beamlines, which are supported by award RR-15301 from the National Center for Research Resources at the National Institutes of Health. Use of the Advanced Photon Source is supported by the US Department of Energy, Office of Basic Energy Sciences under Contract No. DE-AC02-06CH11357.

References

Adams, P. D., Mustyakimov, M., Afonine, P. V. & Langan, P. (2009). *Acta Cryst.* D**65**, 567–573.
Altland, P. D. & Brace, K. C. (1962). *Am. J. Physiol.* **201**, 1188–1190.
Bennett, B., Langan, P., Coates, L., Mustyakimov, M., Schoenborn, B., Howell, E. E. & Dealwis, C. (2006). *Proc. Natl Acad. Sci. USA*, **103**, 18493–18498.
Berenbrink, M. (2006). *Resp. Physiol. Neurobiol.* **154**, 165–184.
Blakeley, M. P., Ruiz, F., Cachau, R., Hazemann, I., Meilleur, F., Mitschler, A., Ginell, S., Afonine, P., Ventura, O. N., Cousido-Siah, A., Haertlein, M., Joachimiak, A., Myles, D. A. A. & Podjarny, A. (2008). *Proc. Natl Acad. Sci. USA*, **105**, 1844–1848.
Blum, M. M., Mustyakimov, M., Rüterjans, H., Kehe, K., Schoenborn, B. P., Langan, P. & Chen, J. C. (2009). *Proc. Natl Acad. Sci. USA*, **106**, 713–718.
Brünger, A. T., Adams, P. D., Clore, G. M., DeLano, W. L., Gros, P., Grosse-Kunstleve, R. W., Jiang, J.-S., Kuszewski, J., Nilges, M., Pannu, N. S., Read, R. J., Rice, L. M., Simonson, T. & Warren, G. L. (1998). *Acta Cryst.* D**54**, 905–921.
Chatake, T., Shibayama, N., Park, S.-H. Y., Kurihara, K., Tamada, T., Tanaka, I., Niimura, N., Kuroki, R. & Morimoto, Y. (2007). *J. Am. Chem. Soc.* **129**, 14840–14841.
Coates, L., Tuan, H.-F., Tomanicek, S, Kovalevsky, A., Mustyakimov, M., Erskine, P. & Cooper, J. (2008). *J. Am. Chem. Soc.* **130**, 7235–7237.
Collaborative Computational Project, Number 4 (1994). *Acta Cryst.* D**50**, 760–763.
Diederichs, K. & Karplus, P. A. (1997). *Nature Struct. Biol.* **4**, 269–275.
Evans, P. (2006). *Acta Cryst.* D**62**, 72–82.
Fisher, S. Z., Kovalevsky, A. Y., Domsic, J. F., Mustyakimov, M., Silverman, D. N., McKenna, R. & Langan, P. (2009). *Acta Cryst.* F**65**, 495–498.
Fisher, S. Z., Kovalevsky, A. Y., Domsic, J. F., Mustyakimov, M., Silverman, D. N., McKenna, R. & Langan, P. (2010). *Biochemistry*, **49**, 415–421.
Hazemann, I., Dauvergne, M. T., Blakeley, M. P., Meilleur, F., Haertlein, M., Van Dorsselaer, A., Mitschler, A., Myles, D. A. A. & Podjarny, A. (2005). *Acta Cryst.* D**61**, 1413–1417.
Helliwell, J. R., Habash, J., Cruickshank, D. W. J., Harding, M. M., Greenhough, T. J., Campbell, J. W., Clifton, I. J., Elder, M., Machin, P. A., Papiz, M. Z. & Zurek, S. (1989). *J. Appl. Cryst.* **22**, 483–497.
International Committee for Standardization in Haematology (1978). *J. Clin. Pathol.* **31**, 139–143.
Kovalevsky, A. Y., Chatake, T., Shibayama, N., Park, S.-Y., Ishikawa, T., Mustyakimov, M., Fisher, S. Z., Langan, P. & Morimoto, Y. (2008). *Acta Cryst.* F**64**, 270–273.
Kovalevsky, A. Y., Chatake, T., Shibayama, N., Park, S.-Y., Ishikawa, T., Mustyakimov, M., Fisher, Z., Langan, P. & Morimoto, Y. (2010). *J. Mol. Biol.* **398**, 276–291.
Kovalevsky, A. Y., Fisher, S. Z., Seaver, S., Mustyakimov, M., Sukumar, N., Langan, P., Mueser, T. C. & Hanson, B. L. (2010). *Acta Cryst.* F**66**, 474–477.
Kovalevsky, A. Y., Hanson, B. L., Fisher, S. Z., Mustyakimov, M., Mason, S., Forsyth, T., Blakeley, M. P., Keen, D. A., Wagner, T., Carrell, H. L., Katz, A. K., Glusker, J. P. & Langan, P. (2010). *Structure*, **18**, 688–699.

Kriebardis, A. G., Antonelou, M. H., Stamoulis, K. E., Economou-Petersen, E., Margaritis, L. H. & Papassideri, I. S. (2007). *Transfusion*, **47**, 1212–1220.
Kroeger, K. S. & Kundrot, C. E. (1997). *Structure*, **5**, 227–237.
Langan, P. & Greene, G. (2004). *J. Appl. Cryst.* **37**, 253–257.
Leslie, A. G. W. (1992). *Jnt CCP4/ESF–EACBM Newsl. Protein Crystallogr.* **26**.
Low, P. S. (1991). *Adv. Exp. Med. Biol.* **307**, 173–183.
Lukin, J. A. & Ho, C. (2004). *Chem. Rev.* **104**, 1219–1230.
Mueser, T. C., Rogers, P. H. & Arnone, A. (2000). *Biochemistry*, **39**, 15353–15364.
Perutz, M. F. (1983). *Mol. Biol. Evol.* **1**, 1–28.
Pflugrath, J. W. (1999). *Acta Cryst.* D**55**, 1718–1725.
Schoenborn, B. (2003). *Trans. Am. Crystallogr. Assoc.* **38**, 40–60.
Sheldrick, G. M. (2008). *Acta Cryst.* A**64**, 112–122.
Tuan, H.-F., Erskine, P., Langan, P., Cooper, J. & Coates, L. (2007). *Acta Cryst.* F**63**, 1080–1083.
Walder, J. A., Chatterjee, R., Steck, T. L., Low, P. S., Musso, G. F., Kaiser, E. T., Rogers, P. H. & Arnone, A. (1984). *J. Biol. Chem.* **259**, 10238–10246.
Waugh, S. M. & Low, P. S. (1985). *Biochemistry*, **24**, 34–39.
Weiss, M. S. (2001). *J. Appl. Cryst.* **34**, 130–135.
Weiss, M. S. & Hilgenfeld, R. (1997). *J. Appl. Cryst.* **30**, 203–205.